ISSN (Print) 1226-1750
ISSN (Online) 2233-6656
Journal of Magnetics 23(4), 499-508 (2018) https://doi.org/10.4283/JMAG.2018.23.4.499

Detailed Magnetic Force Analysis of A 4-Pole Hybrid Electromagnet by Magnetic Equivalent Circuit Method

Hasan Fatih Ertuğrul[1], Kadir Erkan[2]*, and Hüseyin Üvet[2]

[1]*TUBITAK MAM Energy Institute, Gebze, Turkey*
[2]*Yildiz Technical University, Department of Mechatronics Engineering, İstanbul, Turkey*

(Received 23 February 2017, Received in final form 10 December 2018, Accepted 11 December 2018)

In this paper, detailed magnetic force analysis of a 4-pole hybrid electromagnet system providing an advantage of full-redundant levitation is studied. The novel fragmented magnetic equivalent circuit method (MEC) is developed to accurately capture inherited nonlinear characteristics of 4-pole hybrid electromagnet to investigate force characteristics and magnetic field distribution. To confirm this method, two possible scenarios, which are levitation under plain core and levitation under dual-linear motor are composed. As well as, they are examined by both proposed method and FEM analyses. Comparative analyses of both methods revealed that force, inclination torque, and mutual interference can be easily captured with adequate accuracy while at the same time yielding less computation and set up time. Furthermore, the fragmented formulations of permeance functions can be generalized for the analysis and the design of similar devices which specifically involve inclination motions.

Keywords : 4-pole hybrid electromagnet, maglev, magnetic equivalent circuit method, magnetic force analysis, magnetic permanence modeling, 3D-FEM analysis

1. Introduction

Magnetic levitation technology equipped with 4-pole hybrid electromagnets leading to flexible conveyance is one of the potential ways for silent and waste-free, while at the same time, energy efficient operations with low maintenance costs [1-7].

4-pole hybrid electromagnets have the advantages of providing full redundant levitation, multiple-degree of freedom control capability and significantly less power consumption [6]. 4-pole hybrid electromagnet shows inherently nonlinear-coupled force and torque characteristic resulting in instability without active control [5, 6]. Modelling the force characteristics is of crucial importance not only from the viewpoint of control engineering but also from the design and the simulation aspects [8-12].

Several methods of estimating magnetic field distribution and force characteristics of electromechanical devices are presented in literature including analytical, numerical and MEC methods [2-4, 12-20]. Although the analytical methods derived from Maxwell equations are quite powerful tools, they cannot address slot and fringing flux effects. FEM is one of the most extensively used techniques among numerical methods in terms of design and analysis of electromechanical devices due to convenience of commercial availability [9-17]. However, FEM cannot establish a compact functional form of relevance among field distribution, force characteristics and device geometries [18]. Besides, it requires a considerably long set up and computation time. MEC method, in comparison with outlined methods, has a fairly simple theory. It encapsulates slot and fringing effects up to some extent and gives moderate accuracy with less computation time [19-25].

Derivation of permeance functions representing the flux tubes is the initial step in the application of MEC approach. Although the permeance functions of flux tubes having ordinary geometry can be constituted easily as in [2, 3], but in case of complex geometries, it might require more sophisticated approaches, such as conformal mapping, as applied in [19, 20]. Accuracy of MEC method is highly dependent on the modelling of unavoidable slot effects and fringing fluxes. In [17], for an axisymmetric electromagnetic actuator, it has been reported that average flux

*Corresponding author: Tel: +90-507-772-8992
Fax: +90-212-383-2975, e-mail: kerkan@yildiz.edu.tr

error can reduced from 88 % to 67 % by means of precise inclusion of fringing effect. For iron-core linear permanent magnet motors to predict the flux density distribution along with iron losses in high precision is presented with an improved magnetic circuit model to simplify the design process [21-23]. Saturation of ferromagnetic core is another critical issue that must be addressed to get more accurate results when MEC method is applied. A nonlinear equivalent network methodology was investigated and proposed to better predict the electromagnetic performance of hybrid-excited doubly salient electrical machinery [25].

In [5, 6], a simple magnetic equivalent circuit diagram for the 4-pole hybrid electromagnet is given by neglecting the fringing fluxes from the point view of control based dynamical model derivation. In [8], four 4-pole ordinary electromagnets is utilized to construct a maglev based micro manipulation stage. A detailed MEC layout has been developed to analyze and predict the attraction force of ordinary electromagnets by omitting inclination dynamics and torques, since the aim was to obtain micro motion in planar displacements.

In this paper, a detailed air-gap modelling methodology is proposed to enhance the accuracy of MEC method to estimate characteristics of the attraction force, the inclination torques and the mutual interferences for 4-pole hybrid electromagnet. The main contributions of the paper are as follows; the method proposes problem specific permeance functions for 4-pole hybrid electromagnet which is enables the calculation of the inclination torque characteristics and the mutual interferences. These formulations can be generalized for the analysis and the design of similar devices which specifically involves inclination motions. The proposed method is simple to apply and requires less installation and calculation time compared to the existing methods, so the design process is shortened. The calculation time needed to obtain the mutual interference for a specific gap clearance covering full span of both inclinations (α, β) is less than 0.5 seconds for the proposed method and is roughly 2 hours for FEM. The method can be easily implemented in personal computers without the need of any specific software, and various operating conditions can be investigated for 4-pole hybrid electromagnet. In active levitation control design, a rich dynamic model of the system can be derived and the control parametrization for various operating conditions can be easily handled. Furthermore, the MEC model can be used for simulation purposes to observe the performance of the active control and the dynamic behavior of 4-pole hybrid electromagnet in a more accurate manner.

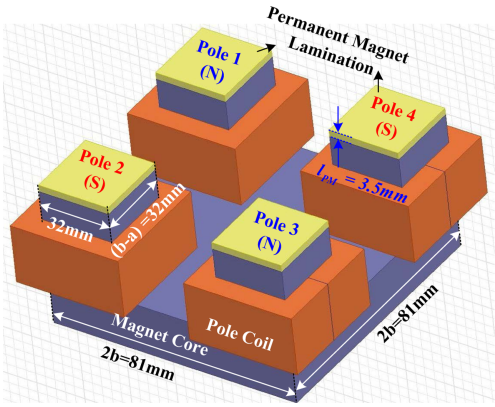

Fig. 1. (Color online) Structural configuration and dimensions of 4-pole hybrid electromagnet.

2. Structure of 4-Pole Hybrid Electromagnet

The 4-pole hybrid electromagnet can be used as a levitating stage to establish a maglev based flexible conveyance system in association with the driving actuators and linear motors. The 4-pole hybrid electromagnet is constructed by combining together 4 magnet poles on a plane with a ferromagnetic core and placing permanent laminations on top of each magnet pole. Fig. 1 shows structural configuration and dimensions of 4-pole hybrid

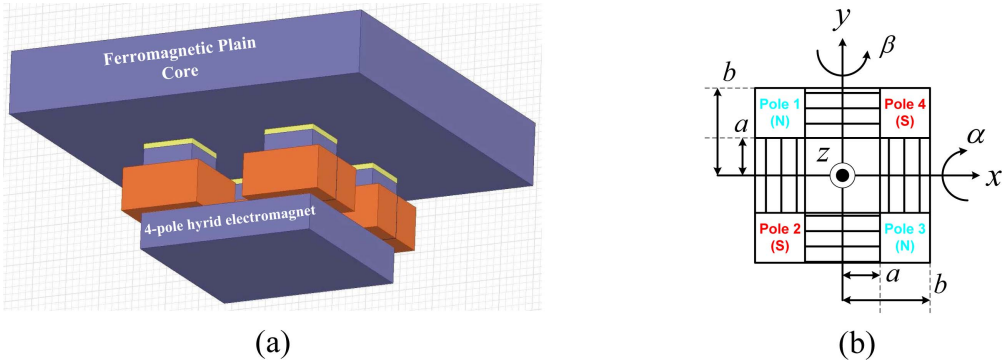

Fig. 2. (Color online) (a) Levitation under the plain core. (b) Axes representation in multi-degree of freedom levitation.

electromagnet. The diagonal poles of the magnet have the same direction of magnetization for the permanent magnet laminations, hence the redundant levitation can be set up readily. In this paper, the levitation of the 4-pole hybrid electromagnet is investigated by two relevant scenarios considering fixed suspension support which are levitation under ferromagnetic plain core, and levitation under dual linear motor.

3. Case 1: Suspension under Plain Core

In the first scenario, it is considered that 4-pole hybrid electromagnet is levitating beneath the ferromagnetic plain core as seen in Fig. 2(a). Axes definitions and geometric relationships are represented in Fig. 2(b). Magnetic equivalent circuit model is developed by considering the following assumptions;

- The magnetic permeability of ferromagnetic body is infinite. (Magnetic reluctance is nearly zero)
- Saturation and hysteresis do not occur in ferromagnetic parts.
- Eddy current in ferromagnetic parts is zero.
- 4-pole hybrid electromagnet has a symmetrical structure.

It is assumed that an abundant amount of fringing fluxes dominantly emerge at the top the magnet poles and loop through the air. Hence, in MEC model development, we have concentrated on precise modelling of air-gap flux distribution while neglecting the ferromagnetic core effects. Two-segment modelling approach is proposed; the first segment including permanent magnet, the side and the corner fringings are modelled by stationary permeance functions. The second segment is then modelled as a dynamic permeance function of air-gap clearance and inclination displacements.

Permeance definitions are illustrated in Fig. 3(a) for the side-view of one pole configuration. The permeance of the permanent magnet (P_{PM}) is a constant value and can be expressed as (1);

$$P_{PM} = \frac{\mu_0 (b-a)^2}{l_{PM}} \tag{1}$$

The side and corner permeances are in ordinary forms and described by (2);

$$P_{si} = \frac{2\mu_0 (\mathrm{a-b})}{\pi} \ln\left(1+\frac{\pi q}{2z}\right)$$
$$P_{cor} = \frac{\mu_0 \pi q^2}{\pi q + 4 l_{PM}} \tag{2}$$

Where q is the fringing distance, a model parameter should be defined properly to get accurate modelling. Dynamic permeance functions representing the second segment of the model are obtained in double integral form by considering equivalent flux path as follows;

$$P_g^1 = \int_{(a-q)}^{(b+q)} \int_{-(b+q)}^{-(a-q)} \frac{\mu_0}{z + y\tan\alpha + x\tan\beta} dxdy$$
$$P_g^2 = \int_{-(b+q)}^{-(a-q)} \int_{-(b+q)}^{-(a-q)} \frac{\mu_0}{z + y\tan\alpha + x\tan\beta} dxdy$$
$$P_g^3 = \int_{-(b+q)}^{-(a-q)} \int_{(a-q)}^{(b+q)} \frac{\mu_0}{z + y\tan\alpha + x\tan\beta} dxdy \tag{3}$$
$$P_g^4 = \int_{(a-q)}^{(b+q)} \int_{(a-q)}^{(b+q)} \frac{\mu_0}{z + y\tan\alpha + x\tan\beta} dxdy$$

The q-parameter is crucial to get accurate results and should be properly added to the integral equations of each pole air-gap permeance model due to motion origin defined as the center of the magnet core. In these formulizations, the superscripts show the corresponding magnet pole and the subscripts represent the medium in which the magnetic pole is defined. Configuration of entire permeances for Pole-1 branch is illustrated in Fig. 3(b). The proposed MEC model of 4-pole hybrid electromagnet is illustrated in Fig. 4(a). Each pole branch consists of stationary and dynamic permeances as well as magnetomotive forces generated by the permanent magnets and the pole windings. Magnetomotive equivalence of a permanent magnet lamination is described as a function of coercivity and length of permanent magnet by;

$$E_{PM} = H_c l_{PM} \tag{4}$$

In each pole branch, the stationary and the dynamic permeances are connected in series as seen from Fig. 4(a). These serially connected permeances can be cast into an

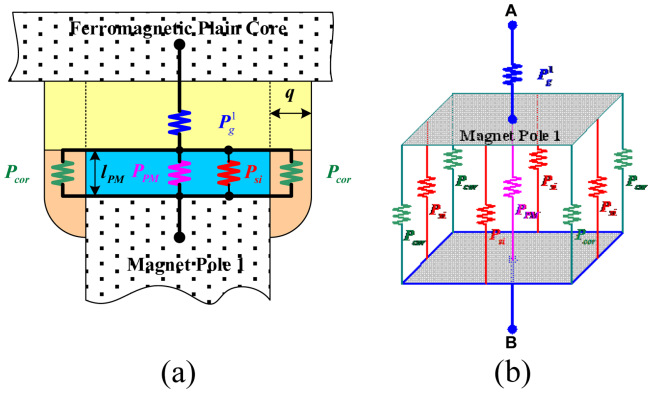

Fig. 3. (Color online) (a) Side-view of one pole-configuration of associated permeances. (b) Representation of equivalent permeances for Pole-1.

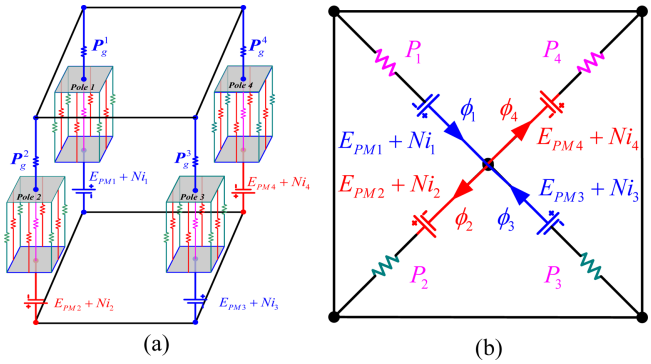

Fig. 4. (Color online) (a) Proposed magnetic equivalent circuit model of 4-pole hybrid electromagnet suspending under the ferromagnetic plain core. (b) Simplified planar configuration of MEC model.

equivalent pole permanence model by proper manipulations as described by following;

$$\begin{aligned} P_1 &= ((4P_{cor}+4P_{si}+P_{PM})P_{gap1})/((4P_{cor}+4P_{si}+P_{PM})+P_{gap1}) \\ P_2 &= ((4P_{cor}+4P_{si}+P_{PM})P_{gap2})/((4P_{cor}+4P_{si}+P_{PM})+P_{gap2}) \\ P_3 &= ((4P_{cor}+4P_{si}+P_{PM})P_{gap3})/((4P_{cor}+4P_{si}+P_{PM})+P_{gap3}) \\ P_4 &= ((4P_{cor}+4P_{si}+P_{PM})P_{gap4})/((4P_{cor}+4P_{si}+P_{PM})+P_{gap4}) \end{aligned} \quad (5)$$

The simplified form of the proposed magnetic equivalent circuit configuration is obtained as in Fig. 4(b). This magnetic circuit can be effectively analyzed by applying any one of magnetic circuit analysis method such as mesh or node to find flux value (φ_i) through each pole branch.

Since the main purpose of this paper is to investigate characteristics of attraction force and inclination torques, one possible approach might be employment of virtual displacement method [1-4]. The energy stored in magnetic field of the 4-pole hybrid electromagnet is given as;

$$W^* = \sum_{k=1}^{4} \frac{1}{2}(E_{PM}+Ni_k)^2 P_k \; ; \; k=1,\ldots,4 \quad (6)$$

Then, the attraction force through z-axis, F_z, and the inclination torques through α and β axes, T_α and T_β respectively, are obtained by taking derivative of the stored energy with respect to corresponding axes variables by following;

$$\begin{aligned} F_z(z,\alpha,\beta,i_z,i_\alpha,i_\beta) &= \frac{\partial W^*}{\partial z}\Big|_{i=const} \\ T_\beta(z,\alpha,\beta,i_z,i_\alpha,i_\beta) &= \frac{\partial W^*}{\partial \beta}\Big|_{i=const} \; ; \\ T_\alpha(z,\alpha,\beta,i_z,i_\alpha,i_\beta) &= \frac{\partial W^*}{\partial \alpha}\Big|_{i=const} \end{aligned} \quad (7)$$

Where the global axes currents (i_z, i_α, i_β) are obtained from actual pole winding currents (i_1, i_2, i_3, i_4) via a current transformation matrix based on stabilizing control of each degree of freedom independently as described in [5, 6]. In this formulation, one of the crucial problems is the calculation of derivatives with respect to axes variables. To eliminate this necessity, an alternative approach employing Maxwell's Tensor formulation is adapted to precisely calculate the attraction force and the inclinations torques [3,26];

$$B_i = \frac{\phi_1}{S_{eq}} \; ; \; f_i = \frac{B_i^2 S_{eq}}{2\mu_0} \; ; \; S_{eq} = ((b+q)(a-q))^2 \; ;$$
$$i = 1,\ldots,4 \quad (8)$$

Once the analysis of the circuit configuration given in Fig. 4 of (a) is performed, the attraction forces induced at each pole is calculated by (8). Then, the total attraction force through z-axis, F_z, and accordingly, inclination torques, T_α and T_β are calculated by the following expressions;

$$\begin{aligned} F_Z &= (f_1+f_2+f_3+f_4) \\ T_\beta &= (f_1+f_2-f_3-f_4)\left(\frac{b-a}{2}+a\right) \\ T_\alpha &= (-f_1+f_2+f_3-f_4)\left(\frac{b-a}{2}+a\right) \end{aligned} \quad (9)$$

To investigate and visually validate the rationality of the proposed modelling approach, 2D and 3D FEM analysis are performed by using Maxwell®-Ansys® commercial package. In all FEM analysis, Steel 1010 is used as the ferromagnetic core material for 4-pole hybrid electromagnet, the plain core and the linear motor core. Table 1 describes the modelling parameters used in analyses.

Figure 5 illustrates 3D field distribution while Fig. 6 demonstrates 2D field distribution of 4-pole hybrid electromagnet for the ferromagnetic plain core and the air-gap. In these analyses, winding currents are set to zero and only permanent magnet excitations are used to energize the MEC. As assumed in the development of magnetic equivalent circuit theory, it can be easily observed from Fig. 5 that the fringing flux-lines dominantly appear in the air-gap circulating the permanent magnets and connecting through the ferromagnetic plain core, hence the rationality of the proposed modelling approach is justified.

Table 1. Model parameters Case I.

a (mm)	8,5	b (mm)	40,5	L_{pm} (mm)	3,5	N (turn)	200
q (mm)	6	z (mm)	6,0	H_c (kA/m)	939		

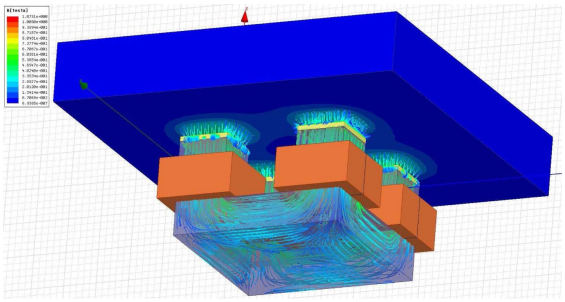

Fig. 5. (Color online) 3-D field distribution plot of the levitation under ferromagnetic plain core.

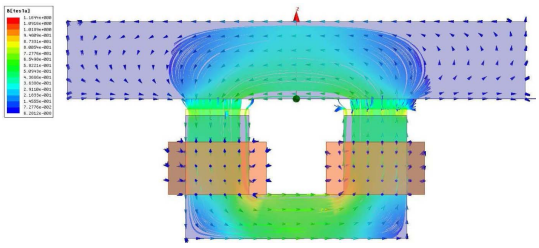

Fig. 6. (Color online) 2-D field distribution plot of the levitation under ferromagnetic plain core.

The first quantitative analysis is carried out on the characteristics of attraction force. Fig. 7 indicates the results of analyses; (a) is for 3D-FEM and (b) is for the proposed model. The MEC structure outlined in previous section is implemented to and executed numerically by employing dblquad function of Matlab®. In the analysis, the geometric dimensions defined in Fig. 1 and Table 1 are used to setup both the FEM and the proposed magnetic equivalent model. The q-parameter is taken as 6mm and thickness of the plain core is equal to width of the hybrid electromagnet pole. The comparison of the results reveal that the proposed model can follow in high accuracy and capture dominant features of 3D-FEM validation-model. The average model error is less than 2 % around operating point z = 7 mm and i_z = 0 A. However, when the operating point is around z = 10 mm and i_z = −5 A, there is a discrepancy between the characteristics. The reason for such an inconsistency is because the flux around the permanent magnet completes its path to the magnet core in a shorter, undesired way without circulating through the plain core. As a result, the force value of FEM is smaller than that of the proposed method.

For α-axis, the relevance among the rotational torque (T_α), axis current (i_α) and the inclination angle (α) is shown in the Fig. 8; (a) stands for 3D-FEM model and (b) stands for the proposed model. The rotational torque characteristic of α-axis is same as the characteristic of β-axis due to symmetrical structure of the 4-pole hybrid electromagnet. As a result, β-axis characteristics will not considered and discussed through the paper. The results of proposed model for α-axis are almost exactly same with the results of the 3D-FEM. The average model error is less than 5 % especially when the operating point is far from α = 0 rad. and i_α = 0 A. The main reason for this inconsistency is due to the fringing flux models in the relatively large air gap clearance. Thus, it cannot capture a fringing flux pattern completing its path in a shorter way through air to the magnet core without circulating the plain core. The results yield that the characteristics in the vertical direction (z) show a highly nonlinear feature, whereas, the characteristics obtained inclination direction (α) represent nearly a linear form which might lead beneficial outcomes for linear control designs.

The mutual interference between each degree of motion freedom is also analyzed. The Fig. 9 shows the effects of

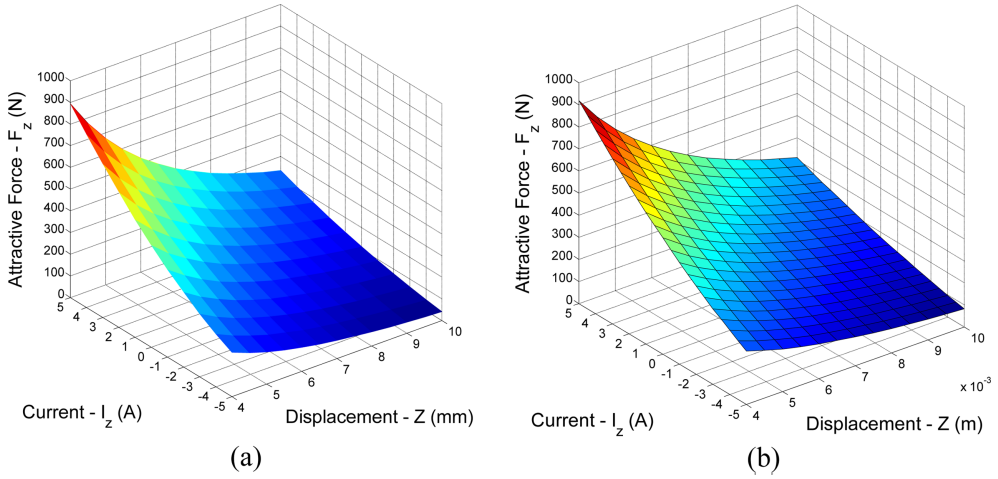

Fig. 7. (Color online) (a) Attraction force characteristic resulted in 3-D FEM analysis. (b) Attraction force characteristic resulted in proposed magnetic equivalent circuit method.

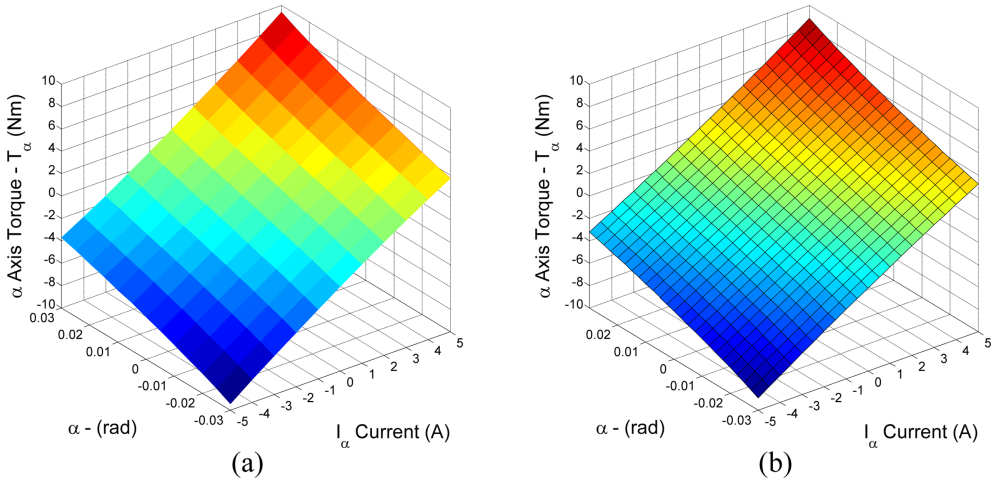

Fig. 8. (Color online) (a) α-Axis inclination torque characteristic by 3-D FEM analysis. (b) α-Axis inclination torque characteristic by proposed modelling approach. (@ z = 10 mm, β = 0 $i_z = i_\beta = 0$)

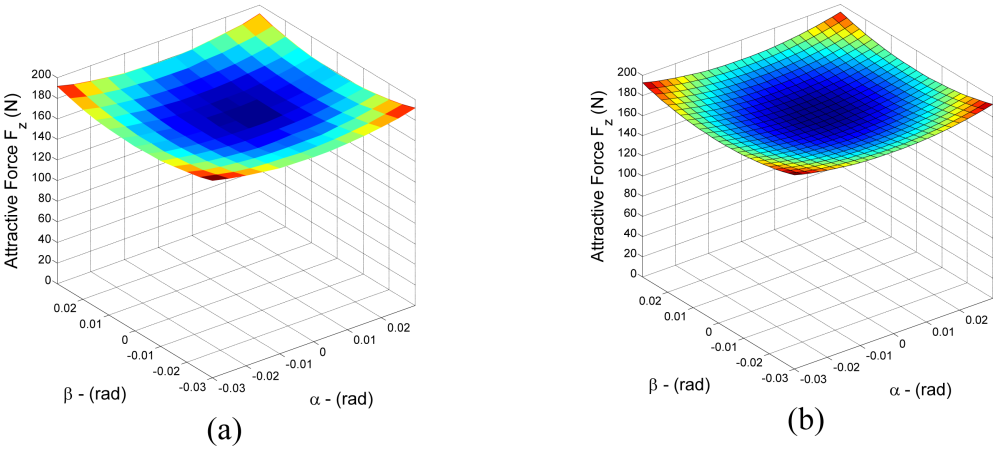

Fig. 9. (Color online) (a) Attraction force characteristic by 3-D FEM analysis. (b) Attraction force characteristic by the proposed approach. (@ z = 8 mm, $i_z = i_\alpha = i_\beta = 0$)

inclination angle on the attractive force (F_z). The FEM result is shown in Fig. 9(a) and the result of proposed model is given in Fig. 9(b). In this situation, the result of proposed model is compatible with FEM. The inclination motions cause a very small deviation in the attractive force. The average deviation of the nominal attractive force is less than 3 % when the inclination angle equals to 0.02(rad). Therefore, the controller design can be fulfilled over each degree of freedom, independently by assuming that the mutual interference is negligible for relatively large air gap.

4. Case 2: Suspension under Dual-Linear Motor

4-pole hybrid electromagnet can be used as moving stage in a driving mechanism such as a linear motor. Two driving configurations can be established by using linear motors as described in [6, 7]. Here, we are going to fulfill our analysis by using dual-motor driving topology. The

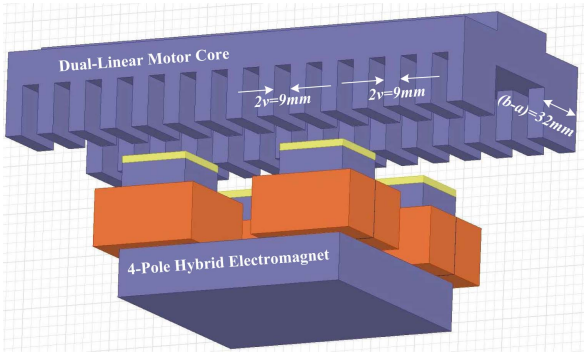

Fig. 10. (Color online) Levitation under dual-linear motor core.

basic structure of dual-motor driving scheme is presented in Fig. 10. 4-pole hybrid electromagnet is suspended under the linear motors, and each motor exerts a driving trust in the same direction to move the electromagnet in a specified course. Since the motor structure has slots which might lead to extra flux paths and fringing, the modelling issue has become more complex than previous case. However, the fragmenting can still be applied to this system with some care.

Flux paths resulted in fringing and as well as slotting effects of linear motor are illustrated in side view form for one of the magnet pole in Fig. 11(a)-(b). Three flux segments are applied to the air-gap, the electromagnet pole and the motor teeth of the system; hence, the modelling effort is remarkably simplified. Top segment is defined over the region of the linear motor tooth and slots. The permeances for *x*-plane and *y*-plane are defined in stationary forms for Pole-1 as following;

$$P^1_{xup} = \frac{2\mu_0(\mathrm{a}-\mathrm{b})}{\pi}\ln\left(1+\frac{\pi v}{2(v/2)}\right),$$
$$P^1_{yup} = \frac{2\mu_0(2v)}{\pi}\ln\left(1+\frac{\pi w}{2(v/2)}\right) \tag{10}$$

These permeances are a function of 4-pole hybrid electromagnet and the motor model parameters (v and w), where w is fringing clearance having the same value as the teeth width for *y*-plane. On the other hand, v parameter is fringing clearance having the same value as the half of the slot width. These permeances have fixed values.

Similarly, bottom segment is specified over the region of the permanent magnets and the air-gap surrounding it within stationary forms. For Pole-1, the permeance functions are described by;

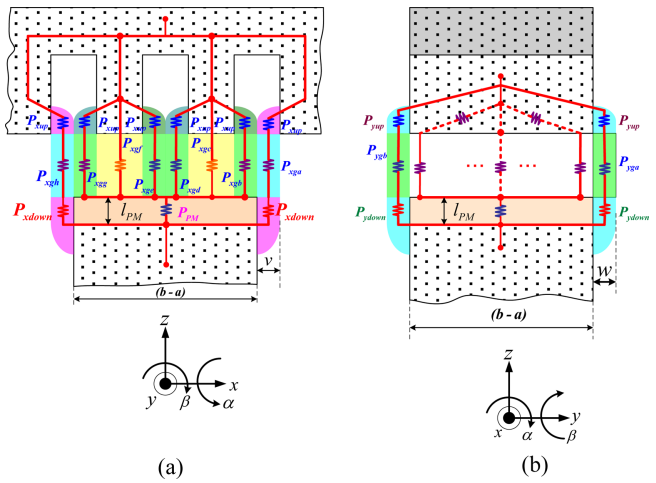

Fig. 11. (Color online) Side-views of a pole-configuration of associated permeances. (a) *y*-plane (b) *x*-plane.

$$P^1_{xdown} = \frac{2\mu_0(\mathrm{a}-\mathrm{b})}{\pi}\ln\left(1+\frac{\pi v}{2l_{PM}}\right),$$
$$P^1_{ydown} = \frac{2\mu_0(2v)}{\pi}\ln\left(1+\frac{\pi w}{2l_{PM}}\right) \tag{11}$$

The middle segment directly captures the air-gap flux paths and is characterized by dynamic permeance functions with proper double integrals as following for *x*-plane and *y*-plane;

$$P^1_{xga} = \int_{(a)}^{(b)}\int_{-(a)}^{-(a-v)} \frac{\mu_0}{z+y\tan\alpha+x\tan\beta}\,dxdy,$$
$$P^1_{xgb} = \int_{(a)}^{(b)}\int_{-(a+v)}^{-(a)} \frac{\mu_0}{z+y\tan\alpha+x\tan\beta}\,dxdy$$
$$P^1_{xgc} = \int_{(a)}^{(b)}\int_{-(a+3v)}^{-(a+v)} \frac{\mu_0}{z+y\tan\alpha+x\tan\beta}\,dxdy,$$
$$P^1_{xgd} = \int_{(a)}^{(b)}\int_{-(a+4v)}^{-(a+3v)} \frac{\mu_0}{z+y\tan\alpha+x\tan\beta}\,dxdy$$
$$P^1_{xge} = \int_{(a)}^{(b)}\int_{-(a+5v)}^{-(a+4v)} \frac{\mu_0}{z+y\tan\alpha+x\tan\beta}\,dxdy, \tag{12}$$
$$P^1_{xgf} = \int_{(a)}^{(b)}\int_{-(a+7v)}^{-(a+5v)} \frac{\mu_0}{z+y\tan\alpha+x\tan\beta}\,dxdy$$
$$P^1_{xgg} = \int_{(a)}^{(b)}\int_{-(a+8v)}^{-(a+7v)} \frac{\mu_0}{z+y\tan\alpha+x\tan\beta}\,dxdy,$$
$$P^1_{xgh} = \int_{(a)}^{(b)}\int_{-(a+9v)}^{-(a+8v)} \frac{\mu_0}{z+y\tan\alpha+x\tan\beta}\,dxdy$$
$$P^1_{yga} = \int_{(a-w)}^{(a)}\int_{-(a+3v)}^{-(a+v)} \frac{\mu_0}{z+y\tan\alpha+x\tan\beta}\,dxdy,$$
$$P^1_{ygb} = \int_{(b)}^{(b+w)}\int_{-(a+3v)}^{-(a+v)} \frac{\mu_0}{z+y\tan\alpha+x\tan\beta}\,dxdy$$
$$P^1_{ygc} = \int_{(a-w)}^{(a)}\int_{-(a+7v)}^{-(a+5v)} \frac{\mu_0}{z+y\tan\alpha+x\tan\beta}\,dxdy, \tag{13}$$
$$P^1_{ygd} = \int_{(b)}^{(b+w)}\int_{-(a+7v)}^{-(a+5v)} \frac{\mu_0}{z+y\tan\alpha+x\tan\beta}\,dxdy$$

Figure 12 illustrates the layout of permeances for one

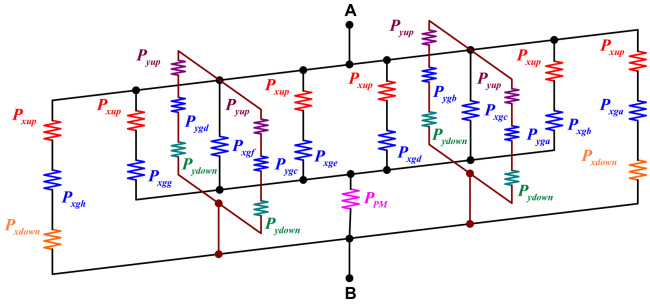

Fig. 12. (Color online) Representation of the equivalent permeances for one magnet pole.

Table 2. Model parameters Case II.

a (mm)	8,5	b (mm)	40,5	L_{pm} (mm)	3,5	N (turn)	200
v (mm)	4,5	w (mm)	9	z (mm)	6,0	H_c (kA/m)	939

pole of 4-pole hybrid electromagnet. Outer branches of the configuration can be further simplified by defining the equivalent permeances as following;

$$P^1_{xud} = \frac{P^1_{xup} P^1_{xdown}}{P^1_{xup} + P^1_{xdown}}, \quad P^1_{yud} = \frac{P^1_{yup} P^1_{ydown}}{P^1_{yup} + P^1_{ydown}} \tag{14}$$

An equivalent permanence value is obtained across the terminals of A and B for one pole configuration by proper manipulation of the circuit components. Moreover, MEC schematic is developed similar to that of the circuit depicted in Fig. 4(b). The MEC method is analyzed as performed in the Case I. As a final step, Maxwell's

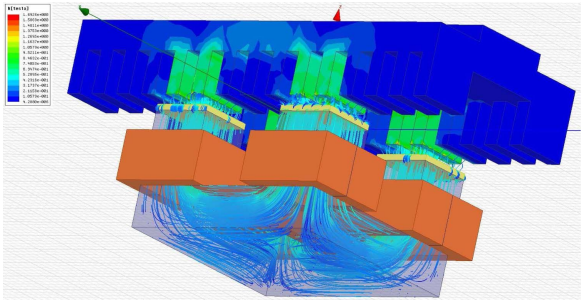

Fig. 13. (Color online) 3-D field distribution plot of the levitation under dual-linear motor core.

Tensor method is applied to calculate the attraction force and rotational torques.

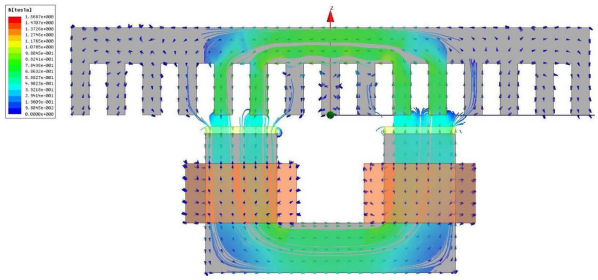

Fig. 14. (Color online) 2-D field distribution plot of the levitation under dual-linear motor core.

3D-FEM analyses are carried out also for this case to validate the effectiveness of the proposed modeling approach. Fig. 13 and Fig. 12 demonstrate the field distribution over the system in 3D and 2D respectively. The definitions of the permeances are consistent with the fringing flux paths as observed from the field plots. In the analyses, the geometric dimensions defined in Fig. 1, Fig. 10 and Table 2 are employed to establish both the FEM and the proposed magnetic equivalent model.

Characteristic of the attraction force is given in Fig. 15; (a) represents FEM analysis and (b) stands for proposed method. As seen from Fig. 15, the proposed model accurately captures the salient features of the FEM validation-model. The average model error can be quantitatively estimated to be less than 2 % for a operating point at z = 7 mm and i_z = 0 A. On the other hand, when the operating point is around z = 10 mm and i_z = –5 A, there is a discrepancy between the characteristics. The main reason of this inconsistency is that the flux around the permanent magnet closes the path to the magnet core in a short way without being circulated through the linear motor core. As

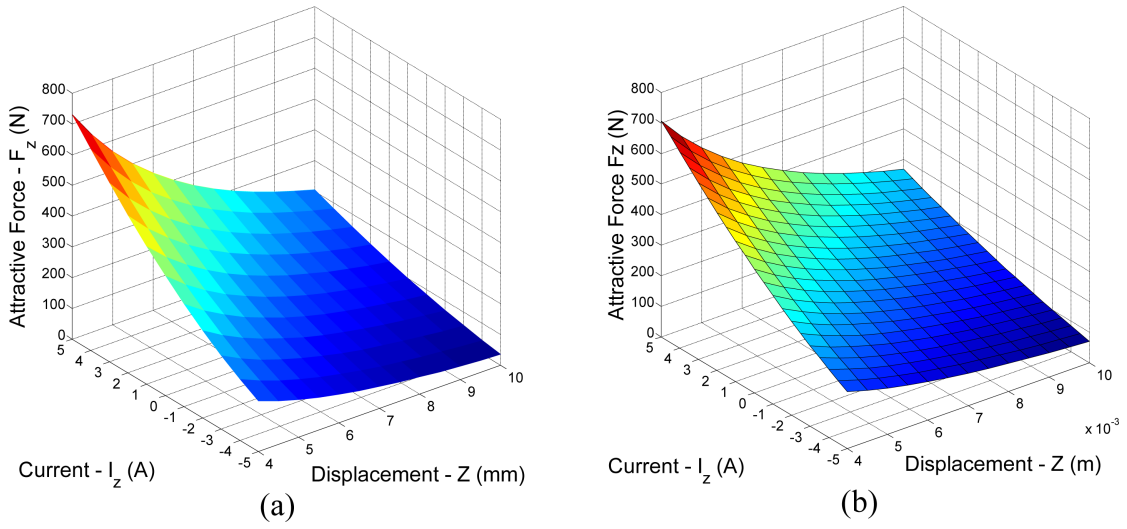

Fig. 15. (Color online) (a) Attraction force characteristic resulted in 3-D FEM analysis. (b) Attraction force characteristic resulted in proposed magnetic equivalent circuit method.

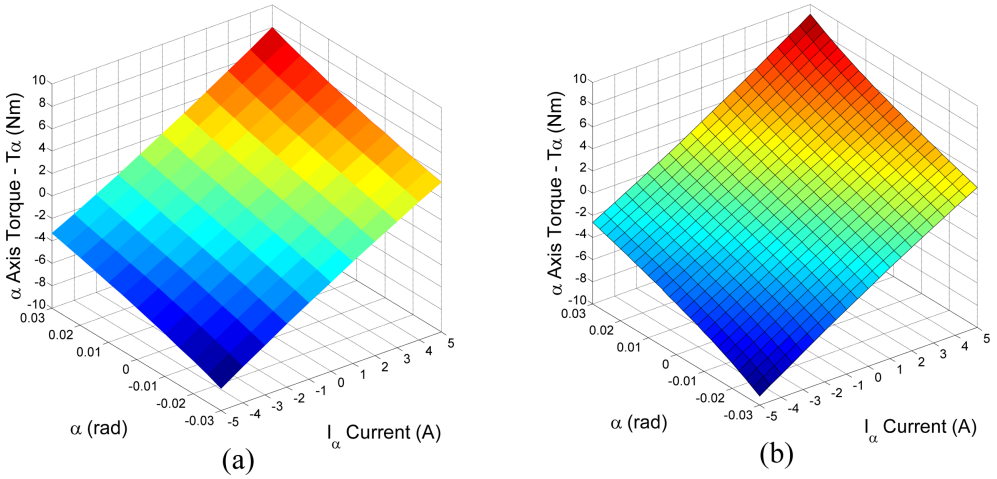

Fig. 16. (Color online) (a) α-Axis inclination torque characteristic by 3-D FEM analysis. (b) α-Axis inclination torque characteristic by proposed modelling approach. (@ z = 10 mm, β = 0, i_z = i_β = 0)

a result, the force value of FEM is smaller than that of the proposed method. Since effective air-gap is decreased by the effect of slots, as comparison with ferromagnetic plain core, the attraction force is reduced in 20 %.

The inclination characteristic describing the relationship among the rotational torque (T_α), axis current (i_α) and rotational displacement (α) is presented in Fig. 16; (a) represents the FEM results and (b) shows the proposed approach. As we have encountered in the Case I; even though the attraction force characteristic exhibits nonlinear attributes, the rotational torque presents almost linear property. It might be quantitatively deduced that the average model mismatch error is smaller than 2 % the operating point around α = 0 rad. and i_α = 0 A.

Moreover, the mutual coupling over the attraction force imposed by rotational displacements is examined as the last analysis. Fig. 17 represents the results of the analysis. The proposed model precisely captures basic properties of FEM validation-model. The rotational displacements cause tiny deviations in the attraction force. So, it might be concluded that the mutual coupling is small enough to be neglected.

5. Conclusion

A precise and straightforward MEC technique based on fragmentation of the air-gap into stationary and dynamic permeances have been proposed and developed for two relevant scenarios of 4-pole hybrid electromagnet.

In the case of levitation under the plain core, the air-gap of each pole was fragmented into two segments; bottom segment was modelled by stationary permanence functions, on the other hand, the top segment was modelled by dynamic permeance functions. The permeances and the magnetomotive forces were properly assembled and the resulting MEC was analyzed.

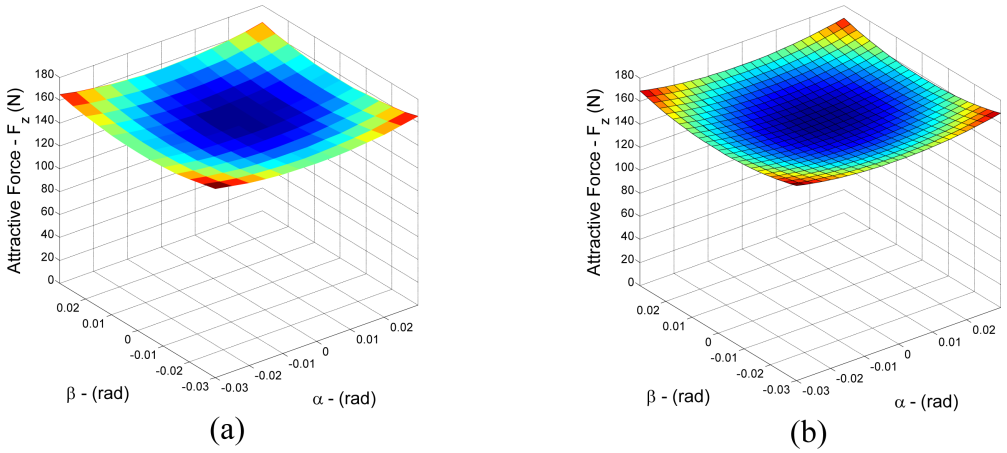

Fig. 17. (Color online) (a) Attraction force characteristic by 3-D FEM analysis. (b) Attraction force characteristic by proposed modelling approach. (@ z = 8 mm, i_z = i_α = i_β = 0)

In the case of the levitation beneath dual-motor core, the air-gap fragmented into three segments; the stationary permeanence functions were used to model the top and bottom segments, whereas the middle segment is solely characterized by dynamic permeance functions. Similarly, MEC was composed and analyzed.

The effectiveness and the accuracy of the proposed MEC method were verified by comparing with FEM results. It has been observed that average model discrepancy error is less than 3 % when the operating point is around z = 8 mm, α = 0 rad., β = 0 rad. and $i_z = i_\alpha = i_\beta = 0$ A. However, if the gap clearance is relatively large, due to the fact that the fringing fluxes complete their path in a shorter way without circulating the plain core or the linear motor core, the model discrepancy error might be as much as 10 %. FEM analyses and the proposed model results reveal the rationality of the proposed method. On the other hand, when the model is set up and the computation times are compared; the computation time required to perform the proposed method is less than 0.5 seconds meanwhile for the FEM analysis it is approximately 2 hours. The design optimization, the control based modelling and the simulation issues of the 4-pole hybrid electromagnet can be solved efficiently with in shorter time and with improved simplicity. Furthermore, the proposed method can be used as a base to accurately estimate the trust induced by the linear motors. The method has introduced specific permeance functions which elaborate the required information to calculate the inclination torque characteristics and the mutual interferences for 4-pole hybrid electromagnet. These formulations can be used for the analysis and design of complex actuators and sensors featuring especially inclination motions.

Acknowledgments

The work was supported by the National Science Foundation of TURKEY (TUBITAK) (No. 112M210).

References

[1] P. K. Sinha, Electromagnetic Suspension: Dynamics & Control, Peregrinus IEE, London (1987) pp 2-56.
[2] J. F. Gieras, Z. J. Piech, B. Tomczuk, and B. Linear, Synchronous Motors: Transportation and Automation Systems, 2nd ed., CRC Press (2011) pp 18-106.
[3] E. P. Furlani, Permanent Magnet and Electromechanical Devices: Materials, Analysis, and Applications, 1st ed., Academic Press (2001) pp 112-116.
[4] I. Boldea, Linear Electric Machines, Drives, and MAGLEVs Handbook, 1st ed., CRC Press (2013) pp 120-327.
[5] J. Liu and T. Koseki, Proceedings of Maglev 2002, Lausanne (2002) pp 83-91.
[6] J. Liu and T. Koseki, International Conference on Electrical Machines and System (ICEMS2001), Jeju (2001) pp 108-113.
[7] T. Koseki, Y. Makino, J. Liu, S. Inui, and Y. Ohira, Proceedings of Linear Drives for Industry Applications, Birmingham (2003) pp 123-126.
[8] K. S. Jung and Y. S. Baek, Mechatronics **13**, 8-9, 981 (2003).
[9] K. Kim, J. Han, C. Kim, J. Lee, and H. Han, Proceedings of IEEE International Conference on Mechatronics and Automation, Beijing (2011) pp 2027-2032.
[10] X. Li, W. Gao, H. Muto, Y. Shimizu, S. Ito, and S. Dian, Precision Engineering **37**, 771 (2013).
[11] H. W. Cho, H. S. Han, J. M. Lee, B. S. Kim, and S. Y. Sung, IEEE Trans. Magn. **45**, 4632 (2009).
[12] Y. D. Du, L. S. Shi, and N. J. Jin, Proceedings of Sixth International Conference on Electrical Machines and Systems (ICEMS 2003), Beijing (2003) pp 563-565.
[13] K. Fujisaki, T. Ueyama, and K. Wajima, IEEE Trans. Magn. **32**, 18 (1996).
[14] D. L. Trumper and J. H. Lang, IEEE Trans. Ind. Appl. **34**, 1254 (1998).
[15] Y. A. Branspiz and A. V. Pastushenko, Proceedings of VIIth International Conference on Mathematical Methods in Electromagnetic Theory, Kharkov (1998) pp 609-611.
[16] D. Atherton and A. Eastham, IEEE Trans. Magn. **10**, 410 (1974).
[17] M. A. Batdorff and J. H. Lumkes, IEEE Trans. Magn. **45**, 3064 (2009).
[18] A. V. D. Bossche, V. Valchev, and T. Filchev, Proceedings of 37th IAS Annual Meeting Conference Record of the 2002 IEEE Industry Applications Conference, Pittsburgh (2002) pp 932-938.
[19] G. A. Cividjian, IEEE Trans. Magn. **45**, 694 (2009).
[20] M. V. Zagirnyak, F. R. Habiunana, and S. A. Nasar, Proceedings IEEE Southeastcon'99, Lexington (1999) pp 197-202.
[21] G. Dajaku and D. Gerling, Proceedings of XIX International Conference on Electrical Machines (ICEM), Rome (2010) pp 1-6.
[22] G. Dajaku and D. Gerling, IEEE Trans. Magn. **46**, 3676 (2010).
[23] B. Sheikh-Ghalavand, S. Vaez-Zadeh, and A. H. Isfahani, IEEE Trans. Magn. **46**, 112 (2010).
[24] L. M. Escribano, R. Prieto, J. A. Oliver, J. A Cobos, and J. Uceda, Seventeenth Annual IEEE Applied Power Electronics Conference and Exposition (Cat. No. 02CH37335); Dallas (2002) pp 144-150.
[25] Z. Zhang, L. Sun, Y. Tao, and Y. Yan, Proceedings of IEEE International Electric Machines & Drives Conference (IEMDC), Chicago (2013) pp 663-669.
[26] H. S. Han and D. S. Kim, Magnetic Levitation: Maglev Technology and Applications, 1st ed., Springer Tracts on Transportation and Traffic (2016) pp 93-98.